Regional Spatiotemporal Statistical Database of Evaporation Ducts Over the South China Sea For Future Long-Range Radio Application

Cheng Yang, *Member, IEEE*, Yafei Shi, *Student Member, IEEE*, Jian Wang, *Senior Member, IEEE*, and Feng Feng, *Member, IEEE*

***Abstract*—To fully grasp the characteristics and provide a basis for establishing an evaporation duct communication system for the South China Sea (SCS), we constructed a regional statistical database based on remote sensing meteorological parameters and a numerical model. This database has the advantage of extensive spatiotemporal coverage and high resolution, which can provide accessibility and as a supplementary means for the maritime sixth Generation communication network. Specifically, work has been completed in three areas. First, the overall evaporation duct height (EDH) in the central SCS varies periodically and remains intense throughout the day, decreasing only just before sunrise during 04:00–08:00. Moreover, a 20.0 m high channel appears at the "Golden edge" in the northern coastal area, which can expand as far as 300 km from the coast during May–July. Second, the characteristics of specific regions were analyzed, and the highest average EDH was determined as 18.4 m in the Taiwan Strait. The height in the central SCS fluctuates little with monthly and annual variation, and it is maintained between 10.0 and 12.0 m. Third, based on the evaporation duct formation principle, we analyzed the spatiotemporal distributions of meteorological parameters. The Taiwan Strait maintains the highest EDH over the SCS, owing to the influence of the Kuroshio Current, and the average sea surface temperature (SST) reaches 28.41°C in June and 19.58°C in January. To the central SCS, high SST, low wind speed, and relative humidity of approximately 80% provide excellent conditions for maintaining an evaporation duct over the long term.**

***Index Terms*—Evaporation duct, spatiotemporal distribution, the South China Sea (SCS).**

Manuscript received 18 June 2022; revised 20 July 2022; accepted 6 August 2022. Date of publication 9 August 2022; date of current version 17 August 2022. This work was supported in part by the National Natural Science Foundation of China under Grant 62031008 and in part by the State Key Laboratory of Complex Electromagnetic Environment Effects on Electronics and Information System under Grant CEMEE2022G0201 and Grant CEMEE-002-20220224. *(Yafei Shi is co-first author.) (Corresponding author: Jian Wang.)*

Cheng Yang and Yafei Shi are with the School of Microelectronics, Tianjin University, Tianjin 300072, China, and also with the Qingdao Institute for Ocean Technology, Tianjin University, Qingdao 266200, China (e-mail: ych2041@tju.edu.cn; shiyafei@tju.edu.cn).

Jian Wang is with the School of Microelectronics, Tianjin University, Tianjin 300072, China, also with the Qingdao Institute for Ocean Technology, Tianjin University, Qingdao 266200, China, also with the Shandong Engineering Technology Research Center of Ocean Information Awareness and Transmission, Qingdao 266200, China, and also with the State Key Laboratory of Complex Electromagnetic Environment Effects on Electronics and Information System, Luoyang 473003, China (e-mail: wangjian16@tju.edu.cn).

Feng Feng is with the School of Microelectronics, Tianjin University, Tianjin 300072, China (e-mail: ff@tju.edu.cn).

Digital Object Identifier 10.1109/JSTARS.2022.3197406

I. Introduction

AN EVAPORATION duct is a peculiar atmospheric phenomenon of the troposphere. It is a type of atmospheric duct with a base layer that extends to the Earth's surface, which is generated by the evaporation of water vapor caused by air-sea interaction under specific meteorological and hydrological conditions. Evaporation ducts frequently occur over the global oceans, their height and intensity vary greatly with longitude, latitude, season, and time of day [1], [2]. It is recognized that an evaporation duct can be considered a layered dielectric duct that supports electromagnetic wave propagation far beyond line-of-sight (BLoS) at specific frequencies with reduced attenuation [3], [4]. Wireless radiowave signals in the ultra-short wave and microwave bands can be transmitted within the atmospheric boundary layer, resulting from a particular atmospheric refractive structure [5]. Variation of meteorological parameters will lead to changes in the radio refractivity and parameters of an evaporation duct [3], consequently, the transmission of a radio system might also be affected [5], [6], [7]. Evaporation ducts might induce specific effects that need further investigation, e.g., adverse impacts, such as radar blind areas and cross-time slot co-frequency interference in mobile communication systems. However, they could also provide new possibilities for BLoS transmission. Therefore, the subject of evaporation ducts has been an area of active research in recent decades [8], [9], [10]. For radio systems based on evaporation ducts, the occurrence and the spatiotemporal pattern of distribution should be fully investigated.

In examining the characteristics and effective use of evaporation ducts, Bean and Dutton [8] revealed the relationship between the atmospheric refraction index and the temperature, atmospheric pressure, and water vapor pressure. Moreover, the research on the prediction of evaporation ducts was performed based on the development of air-sea interaction theory [10], [11]. Hao et al. [12] developed digital maps of atmospheric refractivity and atmospheric ducts based on the processing of radiosonde observation data and surface observation data collected from 2005 to 2014. Focusing on the South China sea (SCS), Lin et al. [13] conducted a statistical study of the region of 0°–40°N, 100°–140°E using ocean and ship data acquired during 1982–1999. Zhao et al. [14] used observational data acquired during atmospheric duct experiments conducted in the

spring during 2010–2012 to complete a statistical analysis of evaporation ducts, surface ducts, and elevated ducts over the SCS and the tropical eastern Indian Ocean. Zhao and Huang [15] analyzed the characteristics of lower atmospheric ducts over the SCS based on global position system radiosonde data acquired during 2006–2012. Shi et al. [16] realized a short-term forecast of the evaporation duct for the west pacific ocean based on the global forecast system. Additionally, Yang et al. [17] constructed a three-dimensional (3-D) mesoscale hydrological and marine meteorological observation network based on oceanic and meteorological observations during cruises and at stations, which has advanced research on air-sea interaction in the SCS. However, the spatiotemporal accuracy and generalization derived from the statistical analyses mentioned above were limited.

The SCS, which is located to the south of the Chinese mainland, is a vast sea area rich in natural resources [18]. The marine economic ecology of the region is undergoing an era of rapid expansion, and the demand for wireless wideband access over the SCS has increased dramatically in recent years. Aims at the future maritime communication system based on the evaporation duct, we proposed a regional statistical method of evaporation duct in the SCS with 0.2° spatial resolution. Furthermore, we constructed a high-resolution, extensive spatiotemporal coverage and 3-D database of evaporation duct characteristics in the SCS. This database is from the latest remote sensing meteorological parameter databases and a numerical model. Additionally, we have analyzed the impact of meteorological factors on evaporation ducts. This constructed database can provide accessibility and as a supplementary means for the maritime sixth Generation communication network [6], [7], [19], [20].

II. Methodology

A. Characteristics of Evaporation Ducts

The density of the tropospheric atmosphere varies both horizontally and vertically, and it exhibits a highly uneven spatial distribution. Consequently, the transmission effect of an electromagnetic signal propagating within the troposphere will change. Moreover, a signal propagating within an atmospheric duct layer will undergo a degree of bending related to atmospheric density, which is usually described by the radio refractivity *N* or the modified refractivity *M* [8]. Radio refractivity is a function of atmospheric temperature, pressure, and water vapor pressure [8], [21]. The modified refractivity can be expressed as $dM/dh = dN/dh + 0.157$, where *h* is the height above the Earth's surface [8]. The degree of bending of an electromagnetic wave is affected mainly by the vertical change of the radio refractivity gradient. The curvature of propagation of an electromagnetic wave bending toward the ground is enhanced when $dN/dh < -0.157$ (i.e., $dM/dh < 0$), which is called super-refraction. In contrast with the propagation of a signal close to the Earth's surface that is commonly limited to line of sight, the energy can be refracted repeatedly within an atmospheric duct layer at appropriate frequencies and angles, so that long-distance transmission can be realized [22].

Atmospheric ducts can be classified as surface ducts and elevated ducts. An evaporation duct is a unique surface duct with the base layer that extends to the Earth's surface, which is mainly caused by the evaporation of seawater. Owing to air-sea interaction, the vertical gradient of humidity varies with altitude [3], [23]. Thus, evaporation ducts have a specific structure that remains within the lower atmosphere, generally just above the ocean surface, and they could play an essential role in supporting long-distance and large-bandwidth transmission of high-frequency signals over the SCS [6], [7], [20].

B. Statistical Method For Evaluation of Evaporation Ducts

1) NCEP Meteorological Datasets: The formation of atmospheric ducts is closely related to the meteorological and hydrological conditions prevalent on different scales. To evaluate the existence of an evaporation duct, it is necessary to measure the structure of the atmosphere and diagnose it according to the modified refractivity. The statistical methods available for such analyses include direct measurements [24], [25], inversion methods [15], [26], [27] and numerical models [28], [29], [30], [31], [32], [33], [34]. Direct measurements mostly get atmospheric parameters of single or multiple positions using a microwave radiometer, gradient meteorological observation, or low altitude atmospheric sounding systems. Therefore, it can be challenging to acquire regional characteristics. Inversion methods realized refractivity structure estimation mainly based on inference from measurements of radar [15], [26] or point-to-point microwave signal strength [27]. Numerical methods obtain duct characteristics by determining the variation of various meteorological parameters with height [35], [36], wide-area, high-resolution, long-term, and near-real-time analyses can be realized by introducing remote sensing data. Currently, public data sources available for the study of evaporation ducts include selected hourly time-series products of the National Centers for Environmental Prediction (NCEP), Climate Forecast System (CFS) [37], European centre for medium-range weather forecasts datasets [38], National Snow and Ice Data Center datasets [39], and National Data Buoy Center datasets [40].

This article selected meteorological parameter datasets from the NCEP CFS version 2 (CFSv2). The National Center for Atmospheric Research and NCEP cooperate to recover observational data from land, the sea surface, ships, radiosondes, aircraft, and satellites [37]. The NCEP CFSv2 was made operational in March 2011, and the related products are available at hourly intervals for the region 0°-359.795°E (the resolution is approximately 0.205° with 1760 grid points), 89.843°N to 89.843°S (the resolution is approximately 0.204° with 880 grid points). The files incorporated in this dataset, which are grouped and updated by month, have been widely used in climatological diagnosis and analysis as a comprehensive meteorological parameter database. In analyzing the characteristics of evaporation ducts, five meteorological parameters need to be considered: the pressure and temperature at the surface, the relative humidity (RH) and temperature at 2 m above the ground and sea surface, and wind speed at 10 m above the surface [41].

2) Naval Postgraduate School (NPS) Model: Numerical methods for evaluating evaporation ducts are generally based on the Monin–Obukhov similarity theory [32], [33]. The variation

of modified refractivity near the sea can be obtained from observational data of hydrometeorological parameters, from which the evaporation duct height (EDH) can be determined. The modified refractivity profile can be analyzed using the Paulus–Jeske model [28], Musson–Gauthier–Bruth model [29], Babin–Young–Carton model [30], and the NPS model [31], and the height and strength of an evaluation duct are obtained.

The applicability of the NPS model has been verified in previous studies [30], [42], [43], [44], and it performed well in matching the measured data [31]. The modified refractivity profile can be calculated from the relationship between temperature, water vapor pressure, and atmospheric pressure. The vertical profile of temperature and specific humidity in the surface layer can be calculated using the following expression [45]:

$$T(z) = T_0 + \frac{\theta_*}{\kappa}\left[\ln\left(\frac{z}{z_{0t}}\right) - \psi_h\left(\frac{z}{L}\right)\right] - \Gamma_d z \quad (1)$$

$$q(z) = q_0 + \frac{q_*}{\kappa}\left[\ln\left(\frac{z}{z_{0t}}\right) - \psi_h\left(\frac{z}{L}\right)\right] \quad (2)$$

where $T(z)$ and $q(z)$ are the air temperature (K) and specific humidity (kg/kg) at altitude z (m), respectively; T_0 and q_0 are the temperature and specific humidity at the sea surface, respectively (with $q_0 = 0.98 q_s(T_0)$, where $q_s(T_0)$ is the sea surface saturated specific humidity calculated from the sea surface temperature (SST) [46]); θ_* and q_* are the Monin-Obukhov specific scale of potential temperature θ (K) and specific humidity q (kg/kg), respectively; κ is the Karman constant; z_{0t} is the thermo-dynamic roughness height; ψ_h is the universal temperature function; Γ_d is the dry adiabatic lapse rate (K/m), which is approximately equal to 0.00976; and L is the similarity length.

The variation of modified refractivity can be obtained by combining the NCEP reanalysis data and the NPS model output. This provides a statistical method for studying the characteristics of evaporation ducts over the SCS.

III. Statistical Characteristics of EDH Over the SCS

A. Spatiotemporal Distribution of EDH

In this article, the EDH over the SCS (5°–25°N, 105°–125°E) was divided in the form of grid points with 0.2° spatial resolution; the value at each position was derived from the hourly meteorological parameters from the NCEP databases and the NPS model output during 2011–2020. Figs. 1–6 shows the spatiotemporal statistical distribution and the lower quartile, median, and upper quartile. The spatiotemporal statistical distribution of the average EDH as a function of hours, months, and years over the SCS is shown in Figs. 1, 3, and 5, respectively. In Figs. 2, 4, and 6, the statistical results with the lower quartile, median, and upper quartile are presented in colored boxes. The remaining values are distributed around the boxes with the "+" sign used to establish the extension line of the colored boxes.

From the various figures, the following conclusions can be drawn as follows.

1) Regional statistical results of evaporation ducts as a function of hours are shown in Fig. 1. To better reveal the patterns between EDH and the alternation between day and night, we considered local time (i.e., Beijing time) rather than UTC. The overall EDH in the central SCS region varies periodically during the day, e.g., around the Xisha Islands, remains intense throughout the day, decreasing only just before sunrise during 04:00–08:00. In the afternoon, the "Golden edge" appears over northern and western coastal areas during 12:00–18:00, when the EDH is higher than in other regions. Influenced by the Taiwan warm current [47], the evaporation duct generally remains intense in the surrounding area of the Taiwan strait. In contrast, the pattern of evaporation intensity in the surrounding area of southeast Asian islands is similar to that in the land area, and the EDH is relatively low.
2) The hourly statistical results are illustrated in Fig. 2. From 05:00, the evaporation from the ocean gradually strengthens with the rising air temperature, and the EDH increases as a result. The EDH increases slowly during the day to reach its highest value (average: 11.1 m) at 17:00. It then decreases gradually overnight to reach its lowest value (average: 9.0 m) at 04:00.
3) From Fig. 3, it can be seen that the EDH over the SCS changes substantially as a function of the month, and the EDH is significantly higher in summer (from June to August) than in other seasons. In terms of spatial distribution characteristics, the monthly statistical pattern over the SCS can be divided into the northern area, central area, and surrounding area of the southeast Asian Islands. Among them, the height in the central SCS remains stable all year round (about 10 m), except in summer when it rises to about 14 m. For the northern SCS, the strength of the duct shows significant seasonal characteristics. From March to July, a duct channel forms around Hainan. A northern coastal channel with a width of $>$300 km forms from March to July. It starts with a small area over the Gulf of Tonkin and then increases toward western regions. In June, the optimal evaporation duct channel forms with a height of $>$20.0 m, connecting Hainan Island and the Taiwan Strait. Then, the height diminishes to $<$10.0 m in September. The distributional characteristics of EDH in the surrounding area of the southeast Asian Islands are unique; a large area with EDH of $>$15.0 m appears over Southeast Asia from December to March. However, the height decreases to $<$5.0 m as the temperature increases.
4) The EDH is higher in the western and eastern coastal areas during January–March, but small over northern coasts. The EDH tends to be higher over the northern coastal area during April–June, while it decreases over lower latitudes. The north coastal channel, which has a width of $>$300 km, forms in June with a height generally $>$20.0 m, and then the height diminishes to $<$10.0 m in September. In winter, the EDH over western and eastern coastal regions gradually increases to over 10.0 m. In terms of spatial distribution characteristics, a large area with EDH of $>$15.0 m appears over Southeast Asia during December–March. However, the height decreases to $<$5.0 m as the temperature increases. During March–July, a duct channel forms around Hainan. It starts with a small area

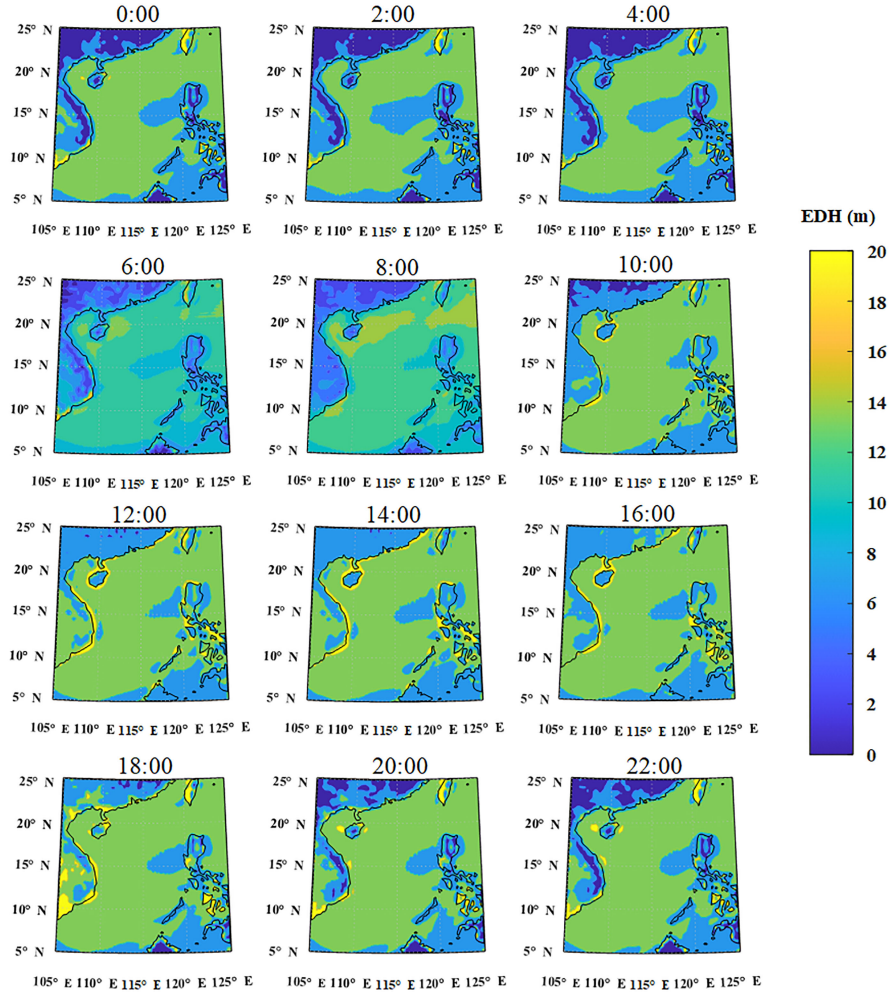

Fig. 1. Regional EDH statistical results in hours (Beijing time: UTC + 08).

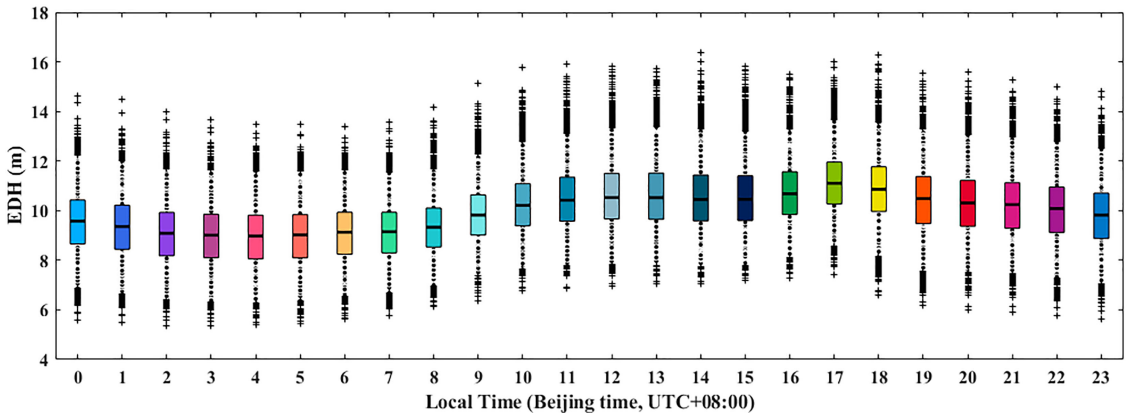

Fig. 2. Hourly statistical results of EDH over the SCS.

over the Gulf of Tonkin and then increases toward western regions. Finally, an evaporation duct channel with a height of >20.0 m forms in June, connecting Hainan and Taiwan.

5) Monthly statistical results are shown in Fig. 4. The EDH is relatively stable in spring and winter. Still, it fluctuates substantially in summer and autumn, indicating the overall form of sinusoidal fluctuation [48]. Compared with other months, it is considerably lower in May, July, and September (the lowest height in September is 8.9 m). The EDH reached its highest value (10.3 m) in June. The

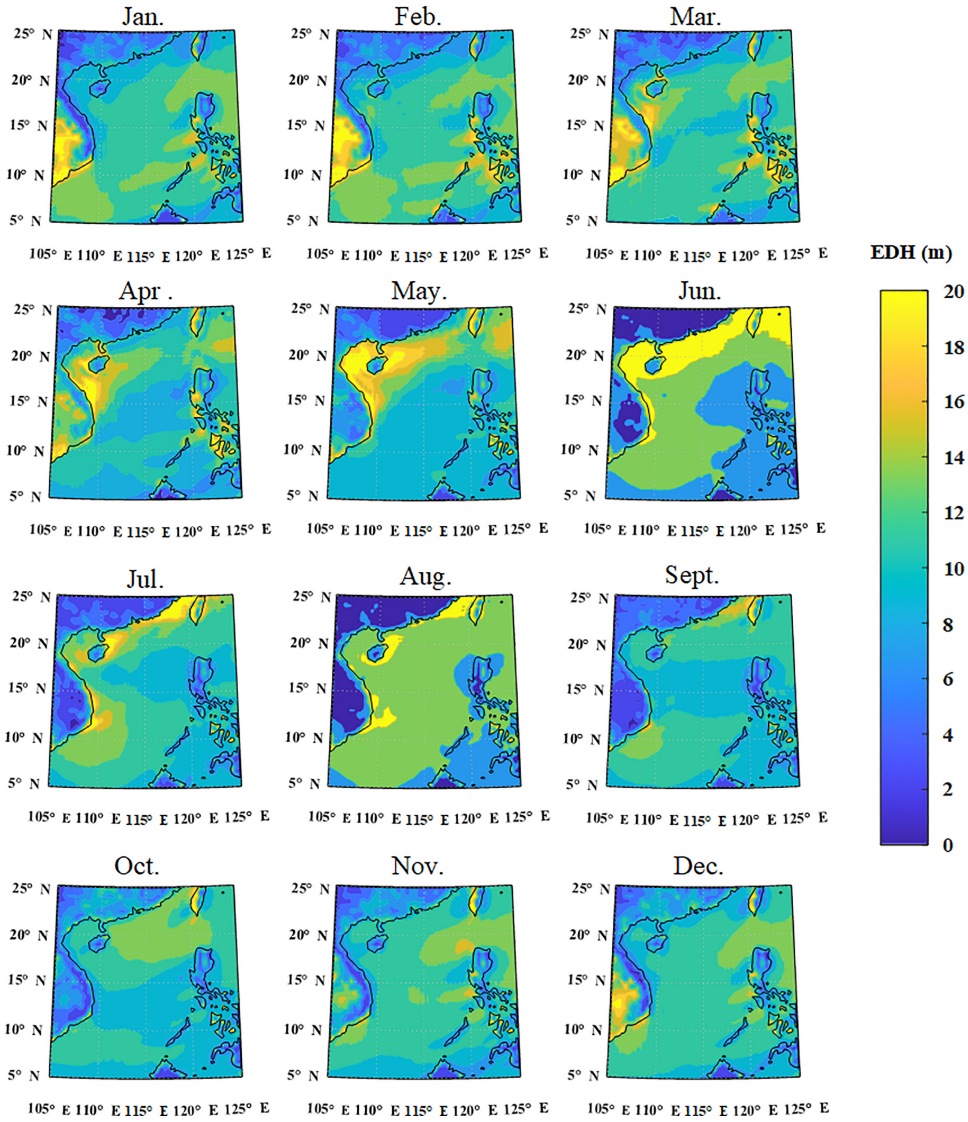

Fig. 3. Regional EDH statistical results in months.

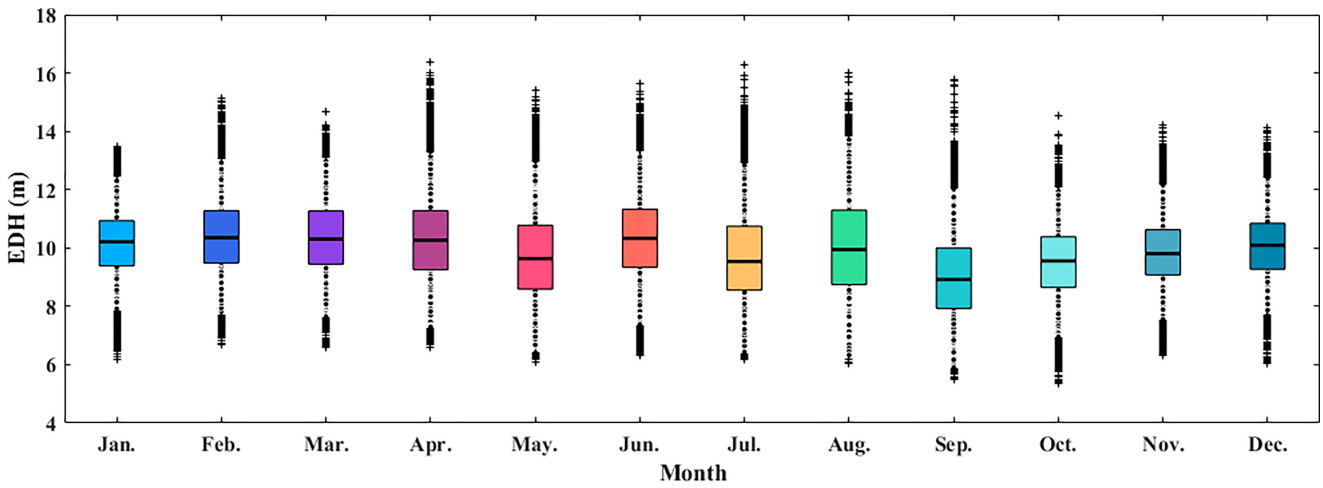

Fig. 4. Monthly statistical results of EDH over the SCS.

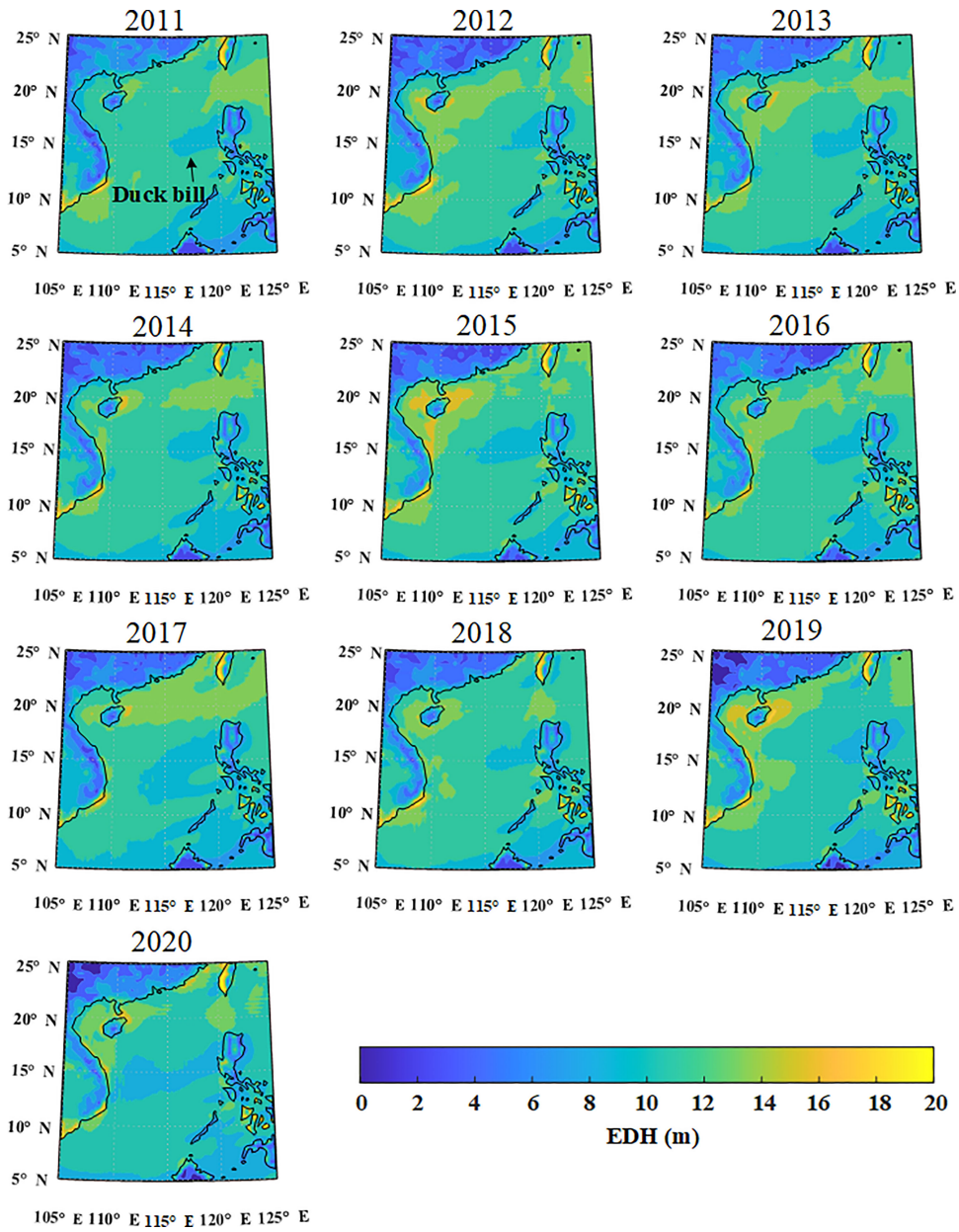

Fig. 5. Regional EDH statistical result in years.

EDH is more condensed and balanced in winter, and the corresponding difference is slight and stable.

6) Fig. 5 shows the annual regional results for the SCS, and the EDH over most of Southeast Asia exceeds 10.0 m. The overall distribution of EDH in the region of the Xisha Islands is between 10.0 and 12.0 m, representing the main level over the SCS. The duct around Hainan shows the most notable annual change over the SCS. It was less active in 2011 when the EDH was between 11.0 and 12.0 m, but the EDH increased in 2015 and 2019 when it exceeded 15.0 m in specific locations.
7) The annual statistical pattern of EDH over the SCS is reflected in Fig. 6. Statistically, the EDH was greater in 2015 and 2019, when the median value was 10.2 and 10.3 m, respectively. The smallest median value over the past ten years was 9.6 m in 2017.

B. Distribution of EDH in Specific Regions of the SCS

The temporal distribution of EDH is not uniform according to the statistical results in different hours, months, and years. Geographically, the SCS has a long-distance coastline to the north and west, islands to the east and south, and a deep sea in the central area, which introduces uncertainty to the EDH. The National Center for Atmospheric Research data from specific regions of the SCS during 2011–2020 were used to analyze the characteristics of EDH, and the statistical results are shown in Fig. 7. The SCS was divided into four specific areas: the

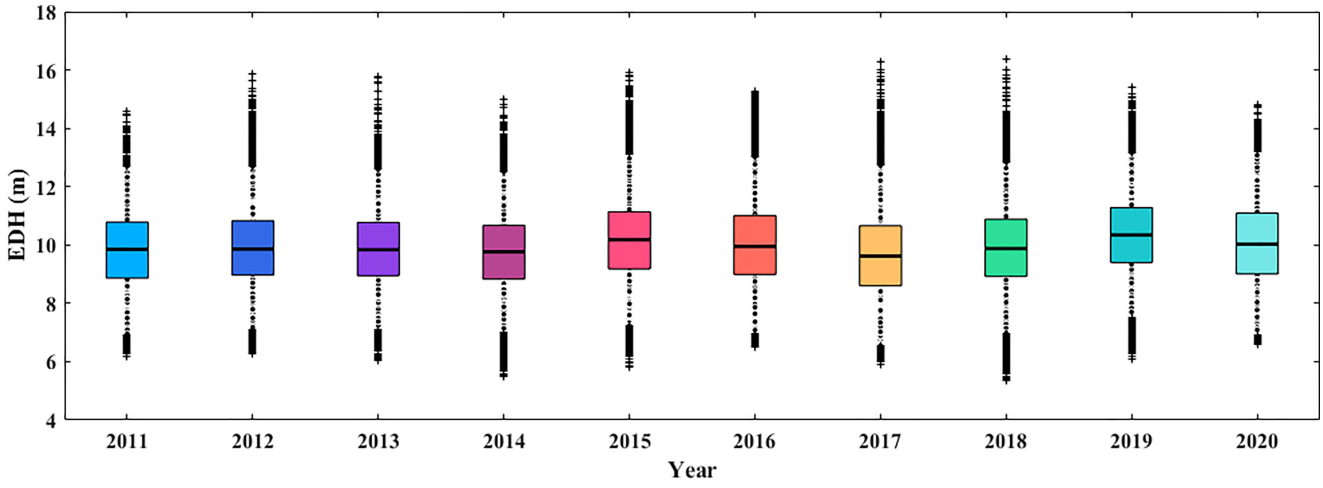

Fig. 6. Yearly statistical results of EDH over the SCS.

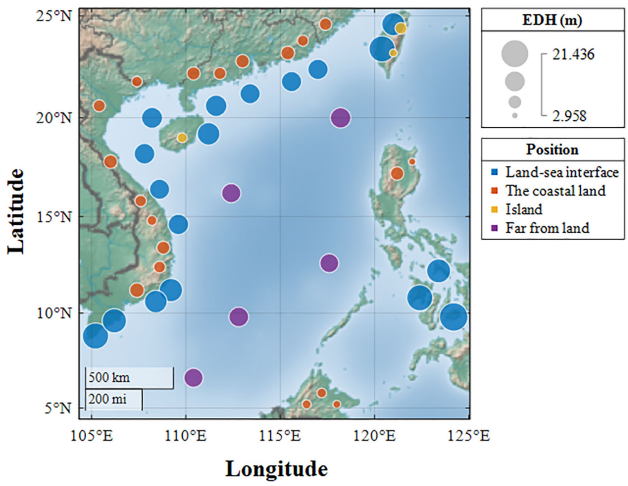

Fig. 7. Statistical results of EDH in the specific regions of the SCS based on National Center for Atmospheric Research data.

land-sea interface; coastal areas; islands; and areas far from land; and the EDH in these specific areas is represented using corresponding circles of different colors and size. The island area shows the lowest EDH (approximately 3.0 m), whereas the highest EDH (18.4 m) is found around the Taiwan Strait in the land-sea interface area. It shows that EDH is most stable in the region far from land and that the overall value of EDH in this area remains high.

Fig. 8 shows the statistical results of EDH in specific regions of the SCS using meteorological data during the past ten years. The following conclusions can be drawn as follows.

1) The EDH over the central SCS fluctuates little with monthly and annual variation, and it is maintained between 10.0 and 12.0 m (average: 11.2 m) over the central SCS.
2) The region of the "northern coastal channel" was selected to represent the land-sea interface area. The prominent feature is that EDH increases from April to August in association with the temperature rises, peaking in June at 19.0 m. It is more uniform in other months with a value of approximately 10.0 m.
3) In the coastal land region, as a function of the month, EDH decreases first and then increases throughout the year. The EDH is higher in spring and winter, reaching the maximum value of 8.1 m in December. The lowest value of 3.4 m was attained in May.
4) The statistical results for the area around Hainan Island represent another typical distribution of EDH over the northern SCS. The average value of EDH is 5.1 m, and the statistical characteristics are generally similar to those of the land-sea interface area but substantially lower. The values of EDH in spring and winter are relatively low, i.e., mostly approximately 3.0 m, but they increase considerably in summer to reach 7.1 m in June.
5) The Taiwan Strait maintains the highest EDH over the SCS, with an annual average height of 18.4 m. Its monthly variation corresponds to a specific statistical distribution pattern of low values in spring and winter and a smooth increase through summer and autumn. The highest EDH of 21.7 m was attained in July.

C. Analysis of the Impact of Meteorological Factors on Evaporation Ducts

1) Analysis of Regional Characteristics: The vertical gradients of meteorological parameters determine the characteristics of an evaporation duct, i.e., the probability of and its strength. The complex ocean currents within the SCS, which include the Kuroshio current (also known as the Japanese current) and the Taiwan current [47], have considerable influence on the characteristics of evaporation ducts. The spatiotemporal distributions of meteorological parameters, including ASTD, wind speed, and RH, were used to analyze the formative factors of evaporation ducts over the SCS. The hourly, monthly, and annual statistical results are shown in Figs. 9–11, respectively. In combination with the statistics results of the EDH, the following conclusions can be derived.

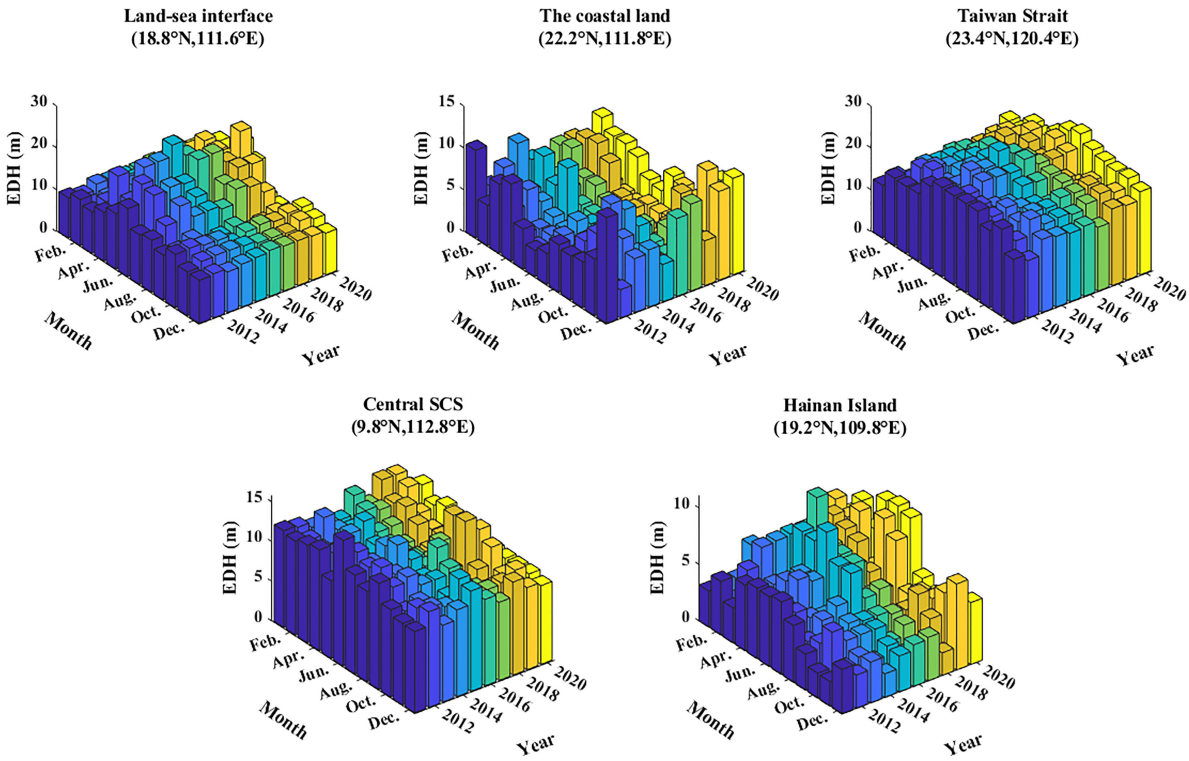

Fig. 8. Statistical results of EDH in specific regions of the SCS based on meteorological data acquired over the past ten years.

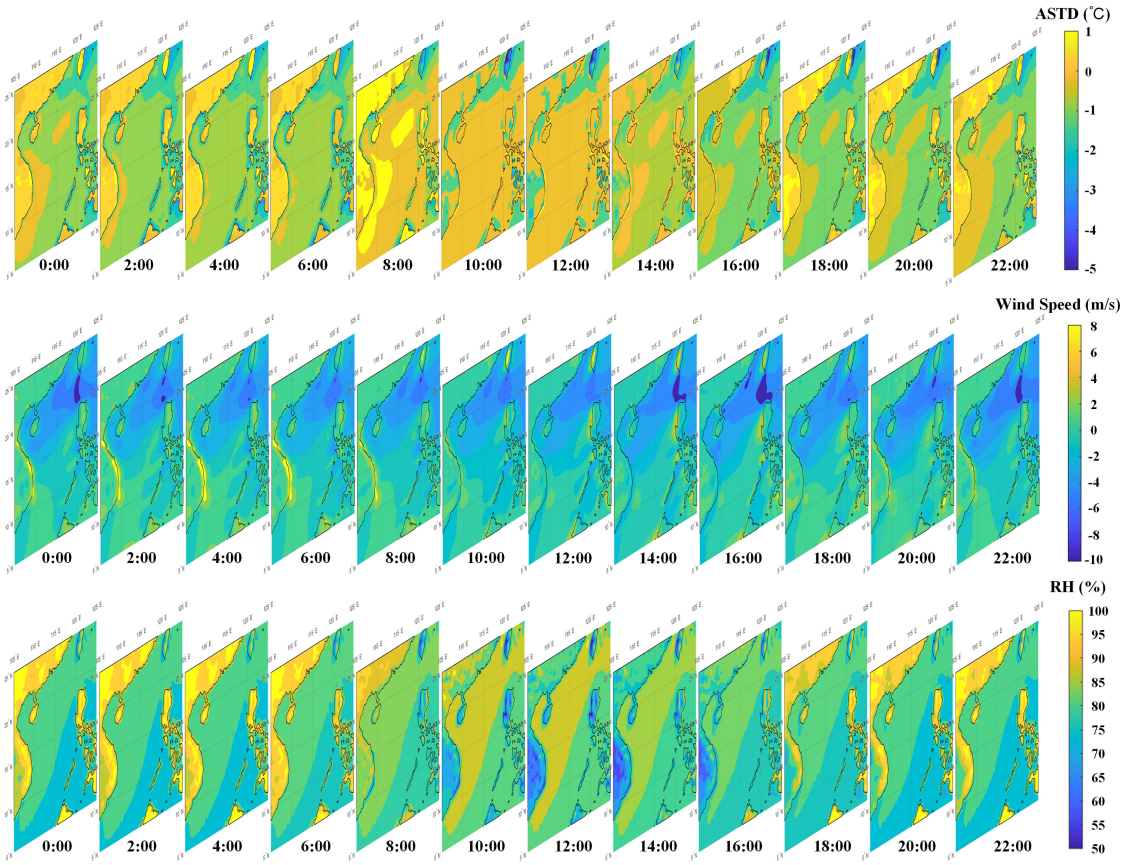

Fig. 9. Regional meteorological parameter statistics in hours (Beijing time: UTC + 08).

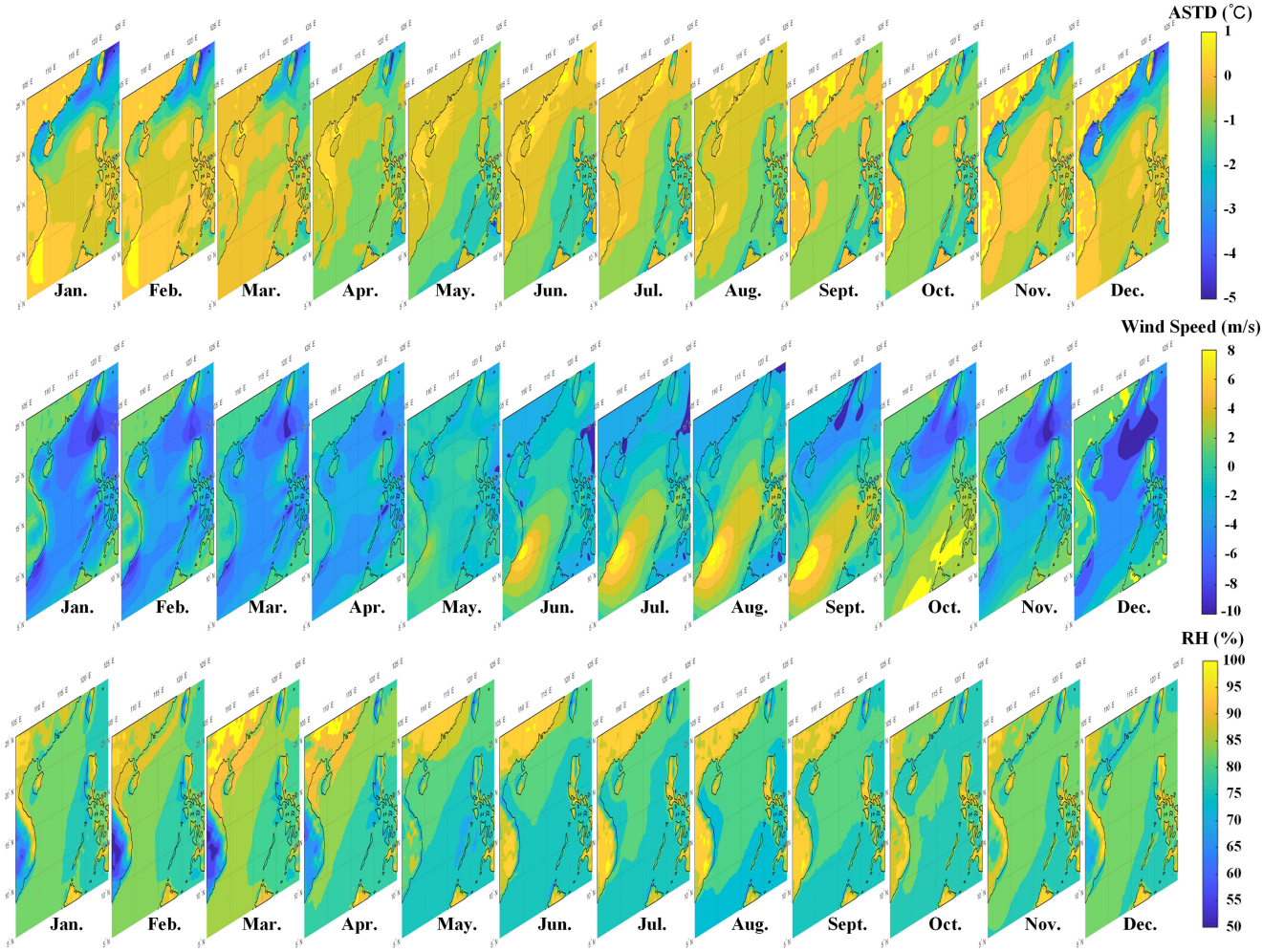

Fig. 10. Regional meteorological parameter statistics in months.

1) Fig. 9 shows a diagram of regional meteorological parameters in hours. The overall wind speed over the SCS is relatively stable, whereas the ASTD and RH vary considerably during 08:00–16:00. The ASTD is >0°C in the coastal areas of western Asia at 08:00, and it largely remains in a neutral or unstable state (ASTD $\leq$ 0) for the remainder of the time. RH increases notably from 08:00 to 14:00, reaching a value of 90% at 12:00 in the northern coastal area, which creates conditions favorable for the enhancement of EDH. The air temperature at night is lower than the SST, and the ASTD is smallest at 06:00, which leads to the lowest EDH. The meteorological characteristics around Hainan Island are more consistent than those of the central SCS. In the afternoon, evaporation ducts over northern and western coastal areas maintain a neutral state. At the same time, the wind speed is generally stable and small (<2 m/s), resulting in the "Golden edge" along the coast, as shown in Fig. 1.
2) In Fig. 10, the meteorological parameters can be generally divided into two phases. In stage I, the central SCS is in a neutral or stable state (ASTD $\geq$0) from November to March, RH is approximately 80%, and the wind speed is low. The northern coastal area is in an unstable state (ASTD <0), and the wind speed is relatively high (>5 m/s), causing the EDH to be maintained at a low level. The central SCS is mainly under neutral and unstable conditions in the second stage from April to October. It maintains a stable and robust condition of RH of approximately 80%, and the SST remains at a high level. The increase in wind speed is the main reason for the high EDH in some regions. After April, the state is neutral or stable, and the EDH begins to rise while the wind speed decreases substantially in the area to the west of Hainan. This trend gradually spreads from the west to the east over time, finally forming a channel over the northern coastal region in June. The ASTD gradually decreases after July, and the EDH slowly decreases as the wind speed strengthens. It is in a neutral or stable state throughout the year over southeast Asia, the wind speed is not high, and RH becomes the decisive factor in determining EDH. RH from January to March is low, which is favorably maintaining the EDH at a high level. After April, the EDH starts to decrease as RH increases.

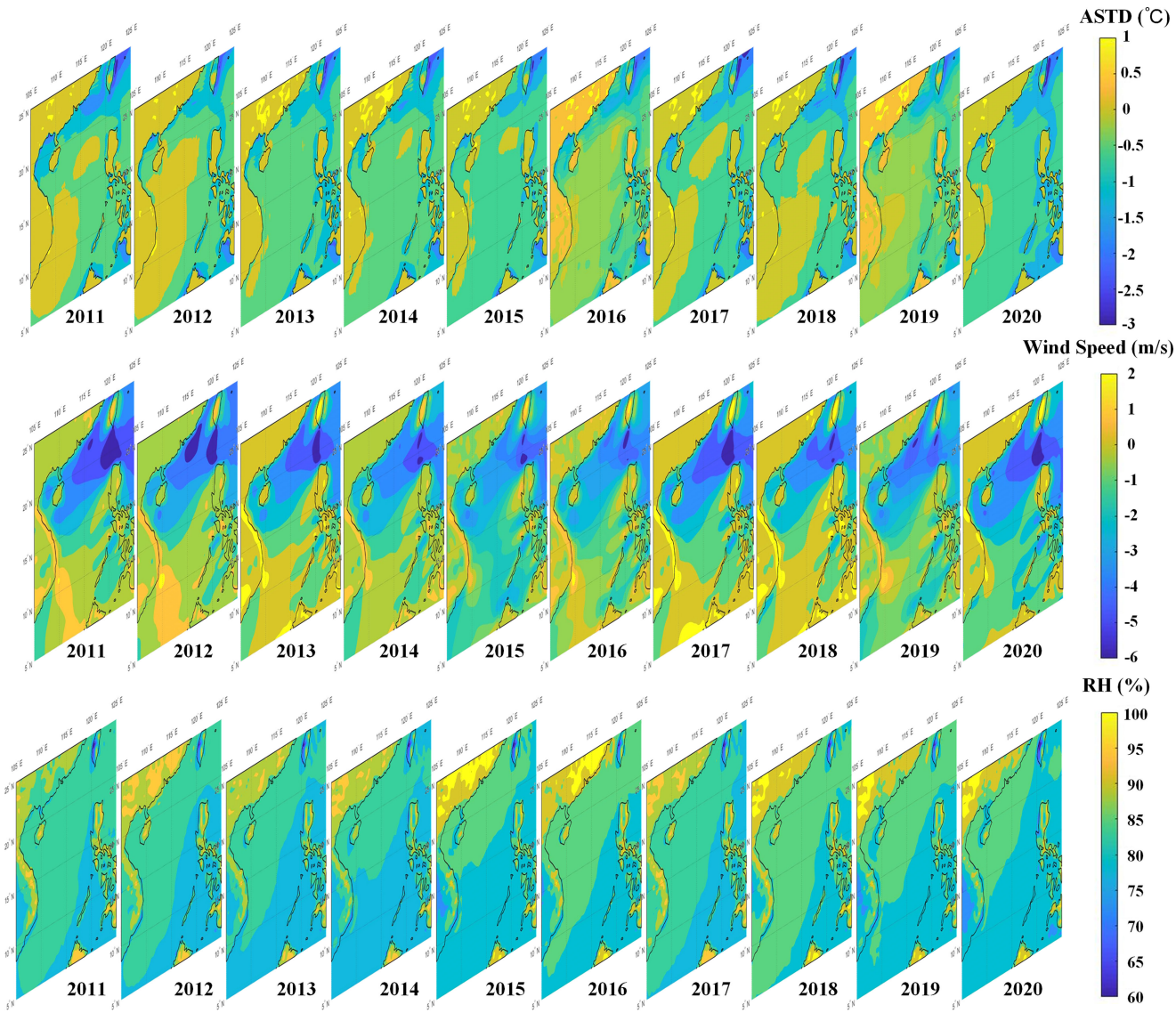

Fig. 11. Regional meteorological parameter statistics in years.

3) According to Fig. 11, the results of the annual characteristics are not prominent. The greatest difference in meteorological parameters is mainly reflected between 2015 and 2019. The overall wind speed of the western coastal area was notably lower than that in other years, and the RH was also reduced. Under a neutral or unstable state, this will result in a specific elevation of the EDH. Influenced by its particular terrain, the northwest region of the Philippines has unique distributional characteristics of current and wind speed that differentiate it from the SCS and also caused the emergence of a "duckbill" shape of EDH in the region to the west of Luzon Island in 2011, as shown in Fig. 5. The near-sea surface around Hainan was mainly stable or neutral in 2015 and 2019, and coupled with the low wind speed and RH in this area, a high evaporation duct was formed.

2) Analysis in Specific Regions: To characterize the distribution of evaporation ducts, meteorological parameters from specific regions during 2011–2020 were collated and displayed in Fig. 12, from which the following conclusions can be drawn.

1) Statistical variations as a function of the hour, month, and year in the regions of coastal land and Hainan Island are similar. The RH distribution around Hainan Island shows the opposite pattern in the other two areas, and it decreases in summer and autumn, resulting in a rise of the EDH. The condition in the region of the coastal land maintains a neutral state, while the wind speed is stable and low (<2 m/s), which is favorable for causing enhancement of EDH when RH decreases in spring and winter.
2) Overall, the meteorological parameters barely change throughout the year, except that RH varies within a small range. It can be seen that SST in the land-sea interface, Taiwan Strait, and central SCS regions is notably high, and the overall ASTD is <0; thus, evaporation of seawater is maintained at a high intensity. The RH in the region of

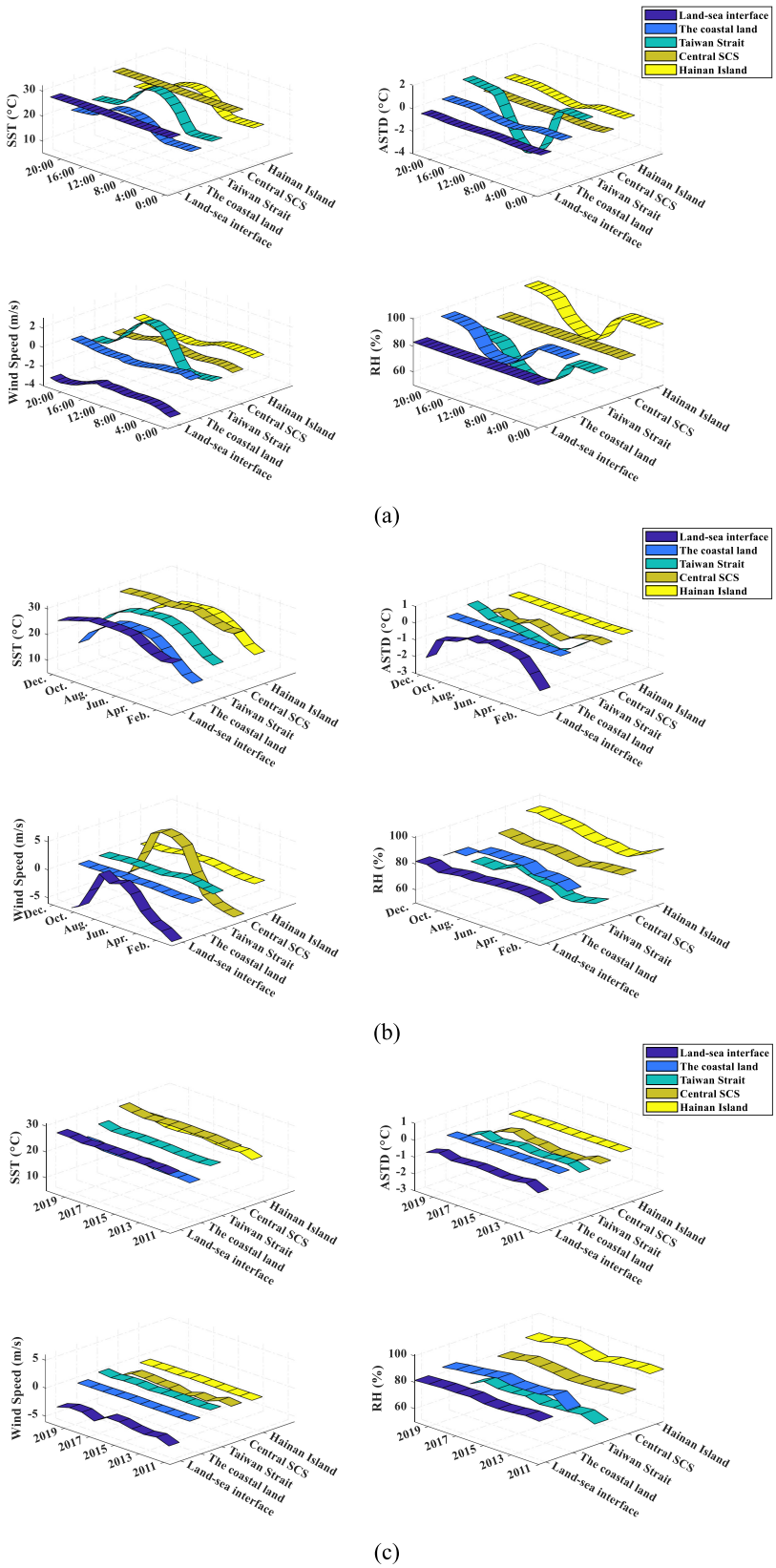

Fig. 12. Meteorological parameter statistics result in specific regions. (a) Statistical results in hours (Beijing time: UTC + 08). (b) Statistical results in months. (c) Statistical results in years.

the Taiwan Strait is low, which is a critical factor for maintaining the EDH at a high level. The average wind speed in the land-sea interface is more significant than that in other regions, leading to the sudden increase of the EDH. Additionally, the variation patterns of meteorological parameters in the coastal land and Hainan Island region are consistent, reflecting similar distributional characteristics of evaporation ducts.

3) Diurnal variation in the land-sea interface region is also not noticeable. In terms of the monthly statistical pattern, wind speed is higher in spring and winter, and RH is generally $<80\%$, which is the principal factor maintaining the EDH at approximately 10 m in winter. With the unstable state in January gradually transitioning to a neutral or stable condition, the wind speed decreases significantly, which indicates enhancement of EDH.
4) Meteorological parameter variations in the region of the Taiwan Strait are stable with daily changes. The SST and wind speed are relatively small at night, and the wind speed and RH increase at sunrise, with the atmospheric boundary layer changing from stable to unstable. After midday, the parameters slowly return to their initial state. The meteorological parameter in this region varies little with month, and the ASTD fluctuates around the neutral state. In the northern sea area, the average SST in the Taiwan Strait reaches 28.41°C in June, owing to the influence of the Kuroshio current [47]. The lowest average SST was 19.58 °C in January. Intense evaporation occurs throughout the year, which is conducive to forming evaporation ducts.
5) The central SCS is in a neutral or stable condition throughout the year, and the influence of wind speed is the main factor that causes the variation of EDH. The parameters of high SST, low wind speed, and RH of approximately 80% provide excellent conditions for maintaining an elevated evaporation duct over the long term.

IV. Conclusion

In this article, a high-resolution spatiotemporal statistical database of evaporation ducts over the SCS was constructed, and the characteristics in specific regions were analyzed. The EDH is highest at 18:00 and lowest at 06:00–08:00, i.e., before sunrise. An evaporation duct channel with a width of >300 km appears over the northern coastal area during May–July, which offers optimal conditions for transmission of electromagnetic signals. The spatiotemporal distributions of meteorological parameters that included ASTD, wind speed, and RH were analyzed. Affected by the land-sea breeze and the Kuroshio Current, in the SCS, the region of the Taiwan Strait has the highest average EDH of 18.4 m.

The regional statistical analysis raised important implications regarding the operation of an evaporation duct communication system and provided auxiliary decision-making information for communication over the SCS [6], [7], [20]. In the future, an experimental communication system using evaporation ducts over the SCS will be constructed based on the preliminary investigation of regional statistical distribution in this article, which may provide accessibility and as a supplementary means for the maritime sixth Generation communication network.

Acknowledgment

The authors also would like to thank the National Center for Atmospheric Research for providing the reanalysis dataset used in this article. The reanalysis data could be obtained through the NCAR public website https://rda.ucar.edu/.

References

[1] C. Liu, Z. Pan, and G. Li, "Statistical analysis of occurrence and characteristics of atmospheric ducts in China," *Chin. J. Radio Sci.*, vol. 11, no. 2, pp. 60–66, Jun. 1996.
[2] Y. Cheng et al., "Observed characteristics of atmospheric ducts over the South China sea in autumn," *Chin. J. Oceanol. Limnol.*, vol. 34, no. 3, pp. 619–628, May 2016.
[3] R. B. Stull, *An Introduction to Boundary Layer Meteorology*. Cham, The Netherlands: Springer, 1988.
[4] L. J. Battan, *Radar Observation of the Atmosphere*. Chicago, IL, USA: Univ. Chicago Press, 1973.
[5] G. S. Woods, A. Ruxton, C. Huddlestone-Holmes, and G. Gigan, "High-Capacity, long-range, over ocean microwave link using the evaporation duct," *IEEE J. Ocean. Eng.*, vol. 34, no. 3, pp. 323–330, Jul. 2009.
[6] C. Yang, J. Wang, and J. Ma, "Exploration of X-Band communication for maritime applications in the South China sea," *IEEE Antennas Wireless Propag. Lett.*, vol. 21, no. 3, pp. 481–485, Mar. 2022.
[7] J. Ma, J. Wang, and C. Yang, "Long-Range microwave links guided by evaporation ducts," *IEEE Commun. Mag.*, vol. 60, no. 5, pp. 68–72, May 2022.
[8] B. R. Bean and E. J. Dutton, *Radio Meteorology*. Atlanta, GA, USA: Tech. Rep. Archive & Image Library, 1966.
[9] J. Choi, "Performance comparison of tropospheric propagation models: Ray-trace analysis results using worldwide tropospheric databases," Nav. Res. Lab., Tech. Rep. NRL/FR/8140-97-9857, Sep. 1997.
[10] M. Ulate, Q. Wang, T. Haack, T. Holt, and D. P. Alappattu, "Mean offshore refractive conditions during Casper-east field campaign," *J. Appl. Meteorol. Climatol.*, vol. 58, pp. 853–874, Apr. 2019.
[11] Q. Jiang, Q. Wang, S. Wang, and S. Gaberek, "Turbulence adjustment and scaling in an offshore convective internal boundary layer: A CASPER case study," *J. Atmos. Sci.*, vol. 77, pp. 1661–1681, Apr. 2020.
[12] X. J. Hao et al., "Digital maps of atmospheric refractivity and atmospheric ducts based on a meteorological observation datasets," *IEEE Trans. Antennas Propag.*, vol. 70, no. 4, pp. 2873–2883, Apr. 2022.
[13] F. Lin, C. Liu, S. Cheng, and Y. Yang, "Statistical analysis of marine atmospheric duct," *Chin. J. Radio Sci.*, vol. 20, no. 1, pp. 64–68, Mar. 2005.
[14] X. Zhao, D. Wang, S. Huang, K. Huang, and J. Chen, "Statistical estimations of atmospheric duct over the South China sea and the tropical eastern Indian Ocean," *Chin. Sci. Bull.*, vol. 58, pp. 2794–2797, Jun. 2013.
[15] X. Zhao and S. Huang, "Estimation of atmospheric duct structure using radar sea clutter," *J. Atmos. Sci.*, vol. 69, pp. 2808–2818, Sep. 2012.
[16] Y. Shi, K. Yang, Y. Ma, Y. Yang, and C. Sun, "Short term forecast of the evaporation duct for the west Pacific Ocean," in *Proc. OCEANS*, 2013, pp. 1–4.
[17] L. Yang et al., "Toward a mesoscale hydrological and marine meteorological observation network in the South China sea," *Bull. Amer. Meteorol. Soc.*, vol. 96, no. 7, pp. 1117–1135, Jul. 2015.
[18] K. Yang, Q. Zhang, and Y. Shi, "Interannual variability of the evaporation duct over the South China Sea and its relations with regional evaporation," *J. Geophys. Res.-Oceans*, vol. 122, no. 8, pp. 6698–6713, Jul. 2017.
[19] J. Wang, C. Yang, and N. Yan, "Study on digital twin channel for the B5G and 6G communication," *Chin. J. Radio Sci.*, vol. 36, no. 3, pp. 340–348, Jun. 2021.
[20] C. Yang and J. Wang, "The investigation of cooperation diversity for communication exploiting evaporation ducts in the South China sea," *IEEE Trans. Antennas Propag.*, to be published, doi: 10.1109/TAP.2022.3177509.
[21] W. L. Patterson, "The propagation factor, fp, in the radar equation," in *Radar Handbook*. New York, NY, USA: McGraw-Hill, 2008.
[22] Q. Wang et al., "Range and height measurement of X-Band EM propagation in the marine atmospheric boundary layer," *IEEE Trans. Antennas Propag.*, vol. 67, no. 4, pp. 2063–2073, Apr. 2019.

[23] A. S. Monin and A. M. F. Obukhov, "Basic laws of turbulent mixing in the surface layer of the atmosphere," *Contrib. Geophys. Inst. Acad. Sci. USSR*, vol. 151, pp. 163–187, Sep. 1954.
[24] W. T. Liu, K. B. Katsaros, and J. A. Businger, "Bulk parameterization of air-sea exchanges of heat and water vapor including the molecular constraints at the interface," *J. Atmos. Sci.*, vol. 36, pp. 1722–1735, Sep. 1979.
[25] X. Hao, L. Guo, L. Lin, Q. Li, and Y. Zhang, "The statistic and analysis of atmospheric ducts worldwide using radiosonde data," in *Proc. 11th Int. Symp. Antennas Propag. EM Theory*, 2016, pp. 911–914.
[26] C. Yardim, P. Gerstoft, W. S. Hodgkiss, and T. Rogers, "Statistical estimation of refractivity from radar sea clutter," in *Proc. IEEE Radar Conf.*, 2007, pp. 938–943.
[27] X. Zhao, "Evaporation duct height estimation and source localization from field measurements at an array of radio receivers," *IEEE Trans. Antennas Propag.*, vol. 60, no. 2, pp. 1020–1025, Feb. 2012.
[28] R. A. Paulus, "Practical application of an evaporation duct model," *Radio Sci.*, vol. 20, no. 4, pp. 887–896, Jul. 1985.
[29] L. Musson-Genon, S. Gauthier, and E. Bruth, "A simple method to determine evaporation duct height in the sea surface boundary layer," *Radio Sci.*, vol. 27, no. 5, pp. 635–644, Sep. 1992.
[30] S. M. Babin, G. S. Young, and J. A. Carton, "A new model of the oceanic evaporation duct," *J. Appl. Meteorol. Climatol.*, vol. 36, no. 3, pp. 193–204, Mar. 1997.
[31] P. A. Frederickson, K. L. Davidson, and A. K. Goroch, *Operational Bulk Evaporation Duct Model For MORIAH Version 1.2*. Monterey, CA, USA: Naval Postgraduate School, 2000.
[32] C. W. Fairall, E. F. Bradley, J. E. Hare, A. A. Grachev, and J. B. Edson, "Bulk parameterization of air-sea fluxes: Updates and verification for the COARE algorithm," *J. Clim.*, vol. 16, pp. 571–591, Feb. 2003.
[33] A. A. Grachev and C. W. Fairall, "Dependence of the monin–obukhov stability parameter on the bulk richardson number over the ocean," *J. Appl. Meteorol. Climatol.*, vol. 36, pp. 406–415, Apr. 1997.
[34] D. A. Newton, *COAMPS Modeled Surface Layer Refractivity in the Roughness and Evaporation Duct Experiment 2001*. Monterey, CA, USA: Naval Postgraduate School, 2003.
[35] W. Zhao et al., "An evaporation duct height prediction model based on a long short-term memory neural network," *IEEE Trans. Antennas Propag.*, vol. 69, no. 11, pp. 7795–7804, Nov. 2021.
[36] X. Zhu, J. Li, M. Zhu, Z. Jiang, and Y. Li, "An evaporation duct height prediction method based on deep learning," *IEEE Geosci. Remote Sens. Lett.*, vol. 15, no. 9, pp. 1307–1311, Sep. 2018.
[37] S. Saha et al., NCEP Climate Forecast System Version 2 (CFSv2) Selected Hourly Time-Series Products. Research Data Archive at the National Center for Atmospheric Research, Computational and Information Systems Laboratory, 2011. Accessed: Dec. 31, 2020. [Online]. Available: https://doi.org/10.5065/D6N877VB
[38] H. Zuo, M. A. Balmaseda, S. Tietsche, K. Mogensen, and M. Mayer, "The ECMWF operational ensemble reanalysis-analysis system for ocean and sea ice: A description of the system and assessment," *Ocean Sci.*, vol. 15, no. 3, pp. 779–808, Jun. 2019.
[39] M. Mcallister, L. Booker, D. K. Fowler, and T. M. Haran, *MODIS Data and Services at the National Snow and Ice Data Center (NSIDC)*. San Francisco, CA, USA: AGU Fall Meeting Abstracts, Dec. 2014.
[40] NDBC PEA, "Programmatic environmental assessment for the national oceanic and atmospheric administration national data buoy center," *Nat. Data Buoy Center*, Jan. 2018. Accessed: Aug. 11, 2022. [Online]. Available: https://www.ndbc.noaa.gov/pea/ndbc_final_pea_20180104.pdf
[41] K. Yang, Y. Ma, and Y. Shi, "Spatio-temporal distributions of evaporation duct for the west pacific ocean," *Acta Phys. Sinica*, vol. 58, no. 10, pp. 7339–7350, May 2009.
[42] Y. Shi, Q. Zhang, S. Wang, K. Yang, and Y. Ma, "Impact of typhoon on evaporation duct in the northwest pacific ocean," *IEEE Access*, vol. 7, pp. 109111–109119, 2019.
[43] S. M. Babin and G. D. Dockery, "LKB-Based evaporation duct model comparison with buoy data," *J. Appl. Meteorol. Climatol.*, vol. 41, no. 4, pp. 434–446, Apr. 2002.
[44] A. A. Grachev, E. L. Andreas, C. W. Fairall, P. S. Guest, and P. O. G. Persson, "SHEBA flux-profile relationships in the stable atmospheric boundary layer," *Bound.–Layer Meteor.*, vol. 124, pp. 315–333, Apr. 2007.
[45] S. D. Burk, T. Haack, L. T. Rogers, and L. J. Wagner, "Island wake dynamics and wake influence on the evaporation duct and radar propagation," *J. Appl. Meteorol. Climatol.*, vol. 42, pp. 349–367, Mar. 2003.
[46] D. P. Alappattu, Q. Wang, and J. Kalogiros, "Anomalous propagation conditions over eastern pacific ocean derived from magic data," *Radio Sci.*, vol. 51, no. 7, pp. 1142–1156, Jul. 2016.
[47] N. Feng, H. Xue, and Y. Fei, "Kuroshio intrusion into the South China sea: A review," *Prog. Oceanogr.*, vol. 137, pp. 314–333, Sep. 2015.
[48] T. Haack and S. D. Burk, "Summertime marine refractivity conditions along coastal California," *J. Appl. Meteorol. Climatol.*, vol. 40, no. 4, pp. 673–688, Apr. 2001.

Cheng Yang (Member, IEEE) received the B.E. degree in electronic and information engineering from Wuhan University, Wuhan, China, in 2012, and the M.S. degree in radio physics from the China Academy of Electronic Sciences, Beijing, China, in 2015, respectively. He is currently working toward the Ph.D. degree in advanced manufacturing with Tianjin University, Tianjin, China.

From 2015 to 2020, he was with the China Research Institute of Radiowave Propagation. His current research interests include microwave radio modeling and electromagnetic environment estimating.

Yafei Shi (Student Member, IEEE) received the B.E. degree in electronic and information engineering from Tiangong University, Tianjin, China, in 2017, and the M.S. degree in radio physics from the China Academy of Electronic Sciences, Beijing, China, in 2020, respectively. He is currently working toward the Ph.D. degree in advanced manufacturing with Tianjin University, Tianjin, China.

From 2020 to 2021, he was with the China Research Institute of Radiowave Propagation. His current research interests include microwave radio modeling and electromagnetic environment estimating.

Jian Wang (Senior Member, IEEE) received the B.S. degree in communication engineering from Hebei University of Science and Technology, Shijiazhuang, China, in 2002, the M.S. degree in the electromagnetic field and microwave technology from China Academy of Electronic Sciences, Beijing, China, in 2005, respectively.

From 2005 to 2019, he was with the China Research Institute of Radiowave Propagation. He is the author of two books, more than 70 articles, and more than 20 inventions. He is currently working with Tianjin University, Tianjin, China. His current research interests include wireless communication and radio channel modeling.

Mr. Wang is currently a Council Member for the China Institute of Command and Control and a Member of the Editorial Board for the *Chinese Journal of Radio Science*.

Feng Feng (Member, IEEE) received the B.Eng. degree in electronic and information engineering from Tianjin University, Tianjin, China, in 2012, and the Ph.D. degree in electromagnetic fields and microwave technology from the School of Microelectronics, Tianjin University, and Electrical and Computer Engineering from the Department of Electronics, Carleton University, Ottawa, ON, Canada, in 2017.

From 2017 to 2020, he was a Post-Doctoral Fellow with the Department of Electronics, Carleton University. He is currently an Associate Professor with the School of Microelectronics, Tianjin University. His research interests include electromagnetic parametric modeling and design optimization algorithms, deep neural network modeling method, space mapping algorithm and surrogate model optimization, the finite element method in electromagnetic simulation and optimization, and Multiphysics modeling and optimization.